THE JOURNAL OF PHYSICAL CHEMISTRY B

Article

pubs.acs.org/JPCB

Substrate Effect on the Plasmonic Sensing Ability of Hollow Nanoparticles of Different Shapes

Mahmoud A. Mahmoud and Mostafa A. El-Sayed*

Laser Dynamics Laboratory, School of Chemistry and Biochemistry, Georgia Institute of Technology, Atlanta, Georgia 30332-0400, United States

Supporting Information

ABSTRACT: Gold hollow nanospheres (AuHSs) and gold hollow nanocubes (AuHCs) were synthesized by the galvanic replacement technique using silver nano templates. Colloidal AuHSs are found to have a higher sensitivity factor than that of AuHCs. This value decreases for both shapes when the nanoparticles are assembled on a quartz substrate by using the Langmuir–Blodgett technique. AuHSs are observed to have the larger effect. It is observed that as the separation gap between AuHCs nanoparticles decreases, their localized surface plasmon resonance band red shifts more than AuHSs. This is accounted for by the discrete dipole approximation (DDA) calculations. The coupling between the plasmon fields of the AuHCs pair is stronger than that between AuHSs pair. Using the DDA calculation, this is found to be due to geometric factors, as well as to the difference in the plasmonic field intensity. The calculation also showed that the plasmon field distributions of both AuHCs and AuHSs were distorted by the quartz substrate in a different manner. It is also observed that the surface-enhanced Raman spectrum of thiophenol is stronger when measured on AuHCs than on AuHSs. This is due to the difference in the plasmon field distribution as well as the fact that the AuHCs have a higher scattering/absorption yield ratio.

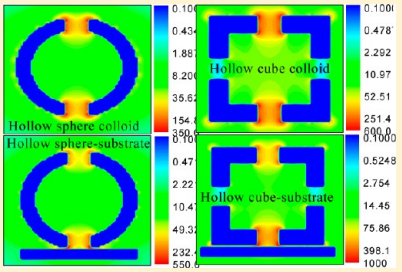

INTRODUCTION

Plasmonic metallic nanoparticles are characterized by the presence of localized surface plasmon resonance (LSPR) and the associated electromagnetic plasmon fields induced when the free electrons oscillate collectively with resonant electromagnetic radiation.[1,2] This plasmon field is generated on the surface of the nanoparticles, which enhances both absorption and scattering. Plasmonic nanoparticles have broad applications utilizing both the LSPR spectrum and the plasmon field.[3] The LSPR and the plasmon field intensity depend on a variety of factors.[4,5] (1) For nanoparticles of similar shapes, a red shift of the LSPR peak is observed as the nanoparticle size is increased.[6] (2) In nanoparticles dimers, the plasmon field coupling between a pair of nanoparticles placed at a separation distance less than twice their size shifts the LSPR peak to a lower energy.[4,7] (3) As the symmetry of the nanoparticles decreases, the LSPR peak red-shifts and a new peak is generated due to the variation of the electron restoring force energy and the polarizability.[3] (4) The LSPR peak red-shifts as the dielectric function of the medium increases.[8] (5) The presence of a substrate distorts the distribution of the plasmon field around the nanoparticles, due to the change of the dielectric function at one side of the nanoparticle, and this either red- or blue-shifts the LSPR peak.[9−11]

Plasmonic nanoparticles of various shapes and sizes have been prepared for different optical or biological applications. The design of the synthesis of the plasmonic nanoparticles is mainly focused on tailoring the LSPR peak position and maximizing the plasmon field intensity. Plasmonic nanoparticles of various shapes such as spheres,[6] cubes,[12] rods,[13] stars,[14] triangles,[15] shells,[16] hollow nanospheres,[17] and frames[18] with LSPR spectrum covering the visible and near-infrared regions have been prepared. Sun and Xia[12] have prepared gold nanocages by galvanic replacement method in which the LSPR peak of these hollow shaped nanoparticles red-shifts as the wall thickness decreases.[19] Two kinds of plasmon fields (inside and outside the hollow nanoparticle) were observed by surface-enhanced Raman spectroscopy (SERS[20]) of thiophenol adsorbed on gold nanoframes and confirmed by discrete dipole approximation (DDA[21]) calculation.[18,22]

Plasmonic nanoparticles have been used in sensing biological systems,[23,24] detecting pollutant gases by SERS,[19] improving optical extinction,[25] and fluorescence techniques.[26] Most of these applications require the nanoparticles to be assembled on the surface of substrate. Different techniques have been used to prepare the plasmonic nanoparticles on the surface of substrate such as electron beam lithography,[27] soft lithography, DC sputtering, nanosphere lithography[2] and helium ion lithography. Although these methods succeeded in preparing different shapes of nanoparticles, the colloidal chemical method remains the most efficient method to control the shape of the nanoparticles. Currently, the difficulties of assembling the colloidal plasmonic nanoparticles on the surface of a substrate limit their applications but the Langmuir–Blodgett technique can overcome this problem. Different shapes of gold and silver

Special Issue: Paul F. Barbara Memorial Issue

Received: August 29, 2012
Revised: October 7, 2012

   dx.doi.org/10.1021/jp3085793 | J. Phys. Chem. B XXXX, XXX, XXX−XXX

nanoparticles have been assembled into monolayers on the surface of both quartz and silicon substrates with controlled interparticle separation.[28,29]

In this paper we study the effect of substrate on the sensing quality of two hollow symmetrical shaped gold plasmonic nanoparticles (spherical and cubic shapes). The bulk LSPR sensing experiment was carried out with hollow gold spheres and gold nanocubes. The LSPR spectra were measured in various solvents for the nanoparticles in colloid and after assembly into Langmuir−Blodgett (LB) monolayers on the surface of quartz substrates at different coverage densities. The spherical and cubic shaped hollow gold nanoparticles were prepared by the galvanic replacement method[12] with silver nanospheres and nanocages used as templates. The comparison of the shift in the wavelength of LSPR peak per unit change of the refractive index of the solvent gives the sensitivity factor of the two shapes of hollow gold nanoparticles. The quality of both spherical and cubic shaped plasmonic nanoparticles in SERS sensing was also examined by comparing the Raman signal of thiophenol vapor adsorbed on the surface of these nanoparticles. To confirm the experimental measurements and understand the substrate effect on the sensing efficiency of the different shaped hollow nanoparticles, DDA calculations of LSPR spectrum and field distribution for both a single nanoparticle and for its dimer placed at different separation gaps were carried out in different solvents.

EXPERIMENTAL SECTION

Hollow gold nanoparticles with cubic (AuHCs) and spherical (AuHSs) shapes were prepared by the galvanic replacement method[12] using the cubic and spherical silver nanoparticles as templates. Silver nitrate, poly(vinylpyrrolidone) (PVP), ethylene glycol (EG), hydrogen tetrachloroaurate ($HAuCl_4$), and thiophenol were purchased from Sigma-Aldrich.

Silver nanospheres (AgNSs) were prepared as follows: In a 100 mL round-bottom glass flask, 50 mL of EG was stirred and heated at 145 °C for 20 min. Then, 0.4 g of PVP (MW ∼ 55 000) was added to the hot EG solution. $AgNO_3$ (0.2. g) dissolved in 5 mL of EG was added at once at a stirring speed of 500 rpm, after which the solution turned yellow due to the reduction of Ag ions into silver particles with a broad LSPR peak around 400 nm. This broad LSPR peak became narrower and blue-shifted with time. The reduction of silver salt was completed after 5 min and the LSPR peak became narrow and located at 402 nm. The AgNSs solution was quenched using ice−water solution. To clean the AgNSs from the byproducts, extra PVP, and organic solvents, 20 mL of AgNSs solution was diluted with 20 mL of acetone and centrifuged for 25 min at 14 000 rpm. The precipitated AgNSs were dispersed in a solution of 0.01 g of PVP dissolved in 100 mL of deionized (DI) water.

Silver nanocubes (AgNCs) were prepared by a modified diol reduction of $AgNO_3$. EG (70 mL) was heated at 140 °C and stirred for 1 h in a 100 mL round-bottom flask. Then 0.8 g of PVP dissolved in 5 mL of EG was added at once to the hot EG and the temperature of the solution was raised gradually until 155 °C. After 5 min, 0.4 mL of 3 mM Na_2S solution in EG was added. Finally, 0.25 g of $AgNO_3$ dissolved in 5 mL of EG was added at once with 200 rpm stirring speed. The resulting solution was stirred for 5 min at 200 rpm until the color changed from brownish yellow to pale yellow; then the stirring and heating were stopped and the solution was shaken vigorously for 5 min. The resulting solution has a LSPR spectrum with intense peak at 414 nm. Cleaning and dispersion of AgNCs were similar to that in the case of AgNSs.

To prepare AuHCs and AuHSs, the cleaned AgNCs and AgNSs solutions in water were heated and brought to boiling. $HAuCl_4$ solution (0.01 g/L) was injected slowly into the hot silver solutions until the LSPR spectrum peak of the solution shifted to ∼630 nm. The AuHCs and AuHSs solutions were refluxed with stirring for 2 min. The solution was cooled and cleaned as reported before. The solution was centrifuged at 10 000 rpm for 5 min and the nanoparticles precipitated down and dispersed in different solvents such as methanol, water, ethanol, THF, chloroform, and carbon tetrachloride for LSPR sensitivity measurements or in chloroform for LB monolayer assembling.

The Langmuir−Blodgett monolayer was prepared as described earlier[22] using a Nima 611D trough; DI water was used as a sublayer. Briefly, 2 mL of AuHCs or AuHSs dispersed in chloroform was sprayed over the water surface and the monolayer was left for 10 min to dry. The LB film was transferred to quartz and silicon substrates by the vertical dipping method at a surface pressure of (0, 0.5, 1, 2, 4, 6, and 8 mN/m. An Ocean Optics HR4000Cg-UV-NIR was used for UV−vis extinction measurements. The optical measurements for the hollow gold nanoparticle monolayers were carried out by fixing the substrates vertically inside a quartz cuvette. A Zeiss Ultra60 scanning electron microscope was used for SEM imaging.

The thiophenol, adsorbed on the surface of nanoparticles by placing the quartz substrates coated with the nanoparticles in a closed container with a small receptacle, was affixed in the center of a Petri dish filled with thiophenol for 2 h. Some of the thiophenol vapor was adsorbed on the surface of particles. A Renishaw Invia Raman microscope with a 532 nm laser was used to measure the Raman spectrum of thiophenol adsorbed on the surface of AuHSs and AuHCsassembled into monolayer on the surface of quartz substrates and collected at different coverage densities.

RESULTS AND DISCUSSION

Characterization of AuHC and AuHS Monolayers. The sensing power of the plasmonic nanoparticles can be recognized by measuring the (1) shift of the LSPR peak after adsorption of an analyte on the surface of the plasmonic nanoparticles,[30] (2) enhancement or quenching of the fluorescence of the analyte by the nanoparticles,[31] and (3) enhancement of the Raman signal of the analyte placed on the plasmon field domain of a nanoparticle. In sensing applications by plasmonic nanoparticles, some requirements should be satisfied. (1) The sensing efficiency of the nanoparticles increases as the strength of the plasmon field increases.[19] The strength of the plasmon field of the plasmonic nanoparticle increases between two coupled plasmonic nanoparticles.[3] However, it has been reported that the plasmon field coupling in hollow-shaped plasmonic nanoparticles dimer at a certain separation gap has a lower plasmon field intensity than that of the single nanoparticle.[22,18] (2) The interparticle distance must not be too small to allow a good interaction between the nanoparticle surfaces and the analyte and to lower the steric hindrance among the adsorbed molecules. (3) The LSPR extinction spectrum is composed of two processes: absorption and scattering.[1] As the size of the nanoparticles increases, the scattering becomes more dominant. For sensing by Raman spectroscopy the scattering is more favorable than absorption. Therefore, the shape and size of the nanoparticles have to be

dx.doi.org/10.1021/jp3085793 | J. Phys. Chem. B XXXX, XXX, XXX−XXX

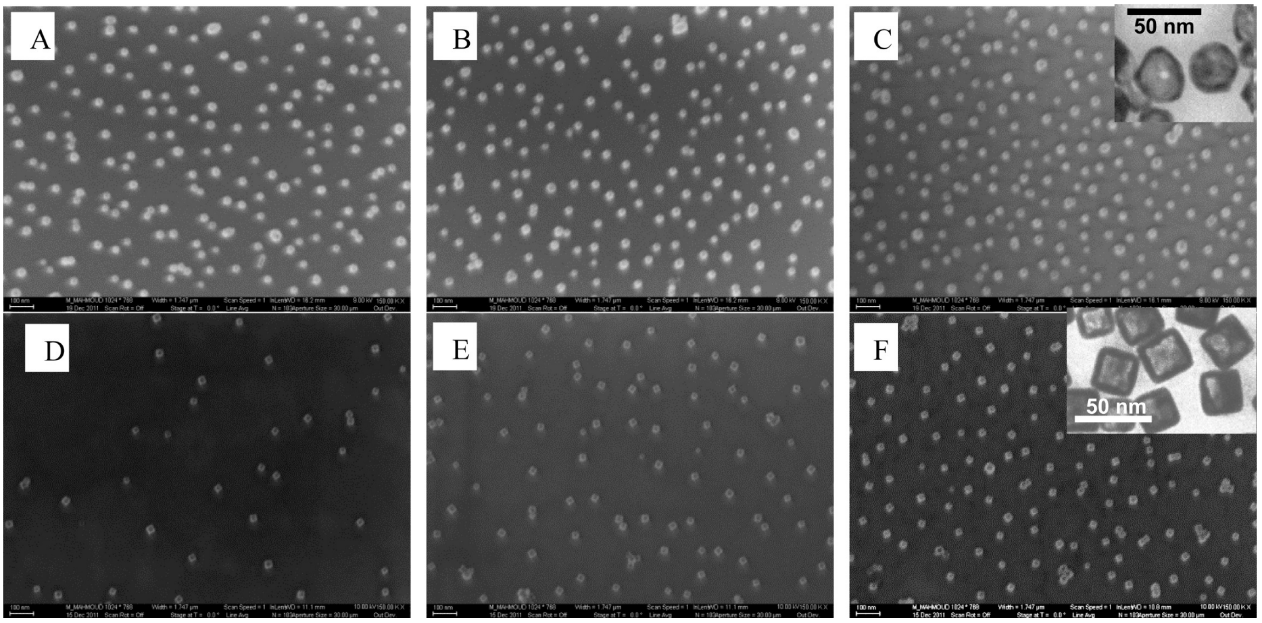

Figure 1. SEM images of AuHSs LB monolayers with densities of coverage of (A) 16.2, (B) 12, and (C) 7.5%. AuHCs monolayers assembled at (D) 13.1, (E) 7.3, and (F) 2% coverage. The scale bar is 100 nm. The insight images are magnified TEM image of AuHSs (top) and AuHCs (bottom).

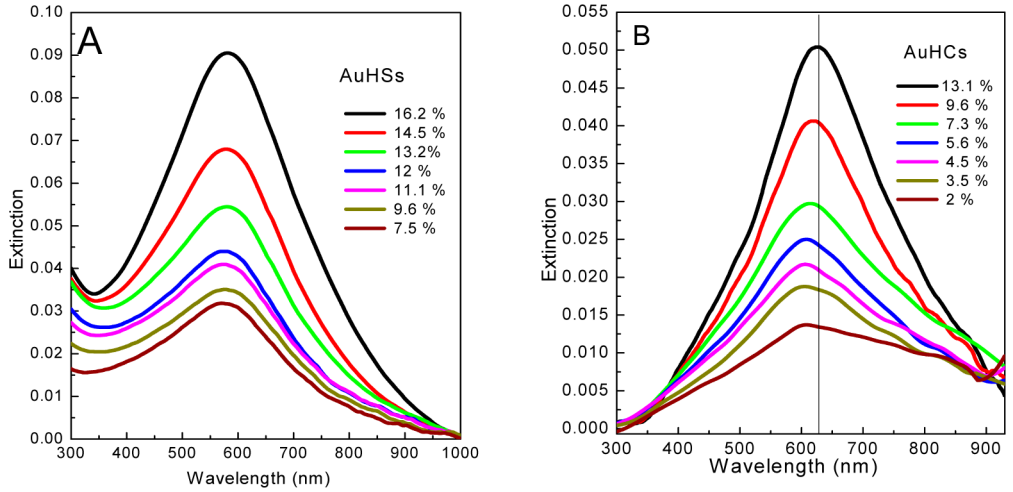

Figure 2. LSPR spectrum of hollow gold nanoparticles assembled into monolayers on the surface of quartz substrate at different percents of coverage. (A) For AuHSs, no observable shift in the LSPR peak as the percent of coverage increases is shown. (B) For AuHCs, the LSPR peak red-shifts as the percent of surface coverage increases.

optimized to obtain high scattering but minimize the destructive interference between the Raman photons and excitation energy dumping.[32] (4) If sensing by Raman spectroscopy, the LSPR has to be in resonance with the wavelength of Raman laser[29] as well as the scattered Raman light. (5) The surface of the nanoparticles has to be clean to increase the surface adsorption on the surface of the nanoparticles and to avoid the interference between the capping and the analyte spectrum or using a capping agent with a low Raman cross-section. (6) The nanoparticles have to be placed at a fixed separation distance before and not during the measurement, because if the interparticle separation distance changes during the measurement, the plasmon field of the individual nanoparticles couples and results in an inaccurate reading. Langmuir−Blodgett (LB) technique is used to assemble the nanoparticles into monolayers in which the interparticle separation distance can be well controlled.[22,33,34]

AuHCs and AuHSs were assembled into LB monolayers at seven different densities of surface coverage. AuHSs were assembled into monolayers by LB technique on the surface of silicon wafer substrates at densities of surface coverage of 16.2, 14.5, 13.2, 12, 11.1, 9.6, and 7.5% (Figure S1, Supporting Information) The surface coverages for AuHCs were 13.1, 9.6, 7.3, 5.6, 4.5, 3.5, and 2% (Figure S2, Supporting Information). Panels A−C of Figure 1 show the SEM images of AuHSs assembled at surface density of 16.2, 12, and 7.5%, respectively. Panels D−F of Figure 1 are the SEM images of AuHCs monolayers with surface coverage of 13.1, 7.3, and 2%.

Hollow shaped plasmonic nanoparticles are characterized by the following properties: (1) The LSPR spectrum red-shifts as the wall thickness decreases.[19] (2) A large surface area results from the presence of inner and outer surfaces.[19] (3) Two kinds of plasmon fields, with different intensities (inner and outer), couple and generate a strong overall plasmon field.[18,22] As the

dx.doi.org/10.1021/jp3085793 | J. Phys. Chem. B XXXX, XXX, XXX−XXX

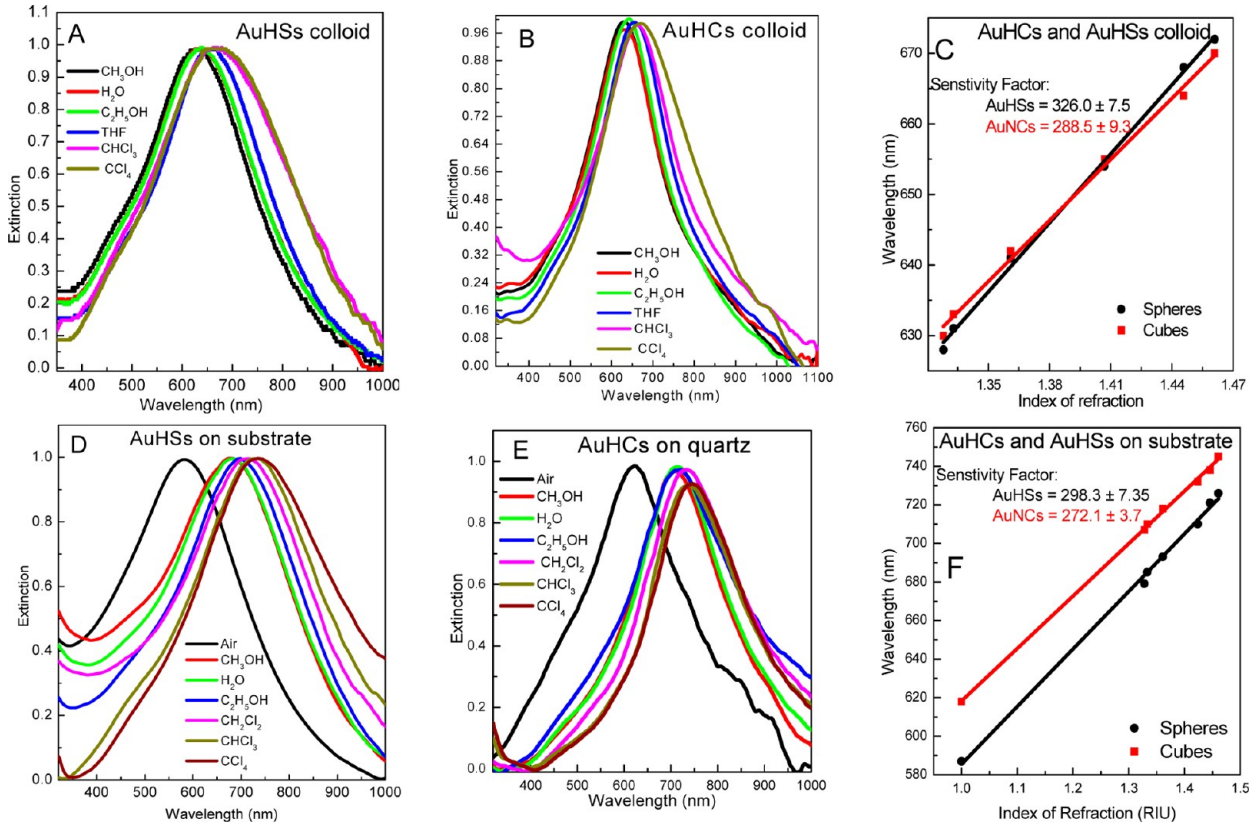

Figure 3. (A) and (B) are the LSPR spectrum of colloidal AuHSs and AuHCs, respectively, measured in different solvents. (D) and (E) are the LSPR spectrum of AuHSs and AuHCs assembled on a quartz substrate at percent of coverage ~7% and measured in different solvents. (C) and (F) are the sensitivity factor linear expression for AuHSs and AuHCs both in a colloid and on a quartz substrate, respectively.

size of the hollow nanoparticles decreases enough, an internal coupling may take place between the inner plasmon fields[18] on facing walls.

Figure 2 shows the LSPR spectra of AuHSs and AuHCs assembled into LB monolayers on the surface of quartz substrates having different coverage densities. The LSPR spectrum peak positions of AuHSs with different densities of coverage are shown in Figure 2A. The LSPR peak of AuHSs with percent of coverage of 7.5% is centered at ~585 nm, and a slight red shift in this peak is observed as the surface coverage density increased from 7.5 to 16.2%. Contradictory to the optical behavior of AuHSs, as the percent of coverage of AuHCs increases, the LSPR peak of AuHCs red-shifted much more than AuHSs (Figure 2B). The LSPR spectrum peaks of AuHCs are at 603 605, 607, 610, 615, 621, and 629 nm when assembled at surface densities of coverage of 2, 3.5, 4.5 5.6, 7.3, 9.6, and 13.1%, respectively. Therefore, the plasmon field coupling between the AuHCs leads to larger red shift in their LSPR peak but not any significant shift for AuHSs.

Substrate Effect on the Sensitivity Factor of AuHCs and AuHSs. The sensitivity factor (SF) is used to express the quality of the plasmonic nanoparticle in LSPR sensing. The SF is defined as the ratio of the shift in the LSPR peak of the plasmonic nanoparticles in "nanometers" per unit change in the refractive index of the surrounding medium. Therefore, the sensitivity factor has the unit nm/RIU. To examine the quality of AuHSs and AuHCs as sensors and to study the effect of the substrate on the sensing efficiency of these two different shapes, the LSPR spectra of these nanoparticles were measured in different solvents. Panels A and B of Figure 3 show the LSPR spectrum of colloidal AuHSs and AuHCs dispersed in different solvents with different dielectric functions. The red shift in the LSPR peak of both the AuHCs and AuHSs were observed as the dielectric function of the medium is increased. Figure 3C shows the linear relationship between the LSPR peaks position of AuHSs and AuHCs and the refractive index of the solvent in which the particles dispersed. The slopes of these straight lines are the sensitivity factors. The SF of AuHSs is found to be 326 ± 7.5 nm/RIU whereas that for AuHCs is 288.5 ± 9.3 nm/RIU. It is interesting to point out that the wall thickness of the sphere here is 4 nm and that of the cage is 5 nm.

The position of the LSPR of AuHSs and AuHCs assembled on the surface of quartz substrate with percents of coverage of 7.5 and 7.3%, respectively, were measured in solvents with different dielectric functions. The optical measurements were carried out for AuHS and AuHC monolayers on quartz substrate that was immersed vertically into the solvents. The sensitivity factor of the AuHSs and AuHCs, calculated from the slope of linear expression, are 298.3 ± 7.35 and 272.1 ± 3.7 nm/RIU (Figure 3F), respectively. After transferring AuHSs and AuHCs to a quartz substrate surface, their sensitivity factors were decreased by 8.6 and 6%, respectively. Thus, the quartz substrate decreases the sensitivity factors of both the hollow spheres and hollow cubes but more significantly affects the spheres. Moreover, the LSPR peaks of the AuHSs and AuHCs on the quartz substrate are red-shifted with respect to the equivalent colloidal particles regardless of solvent.

Sensitivity Factors of AuHCs and AuHSs by Calculation. To explain the experimental results of the sensitivity factor measurements of AuHSs and AuHCs and to study the

dx.doi.org/10.1021/jp3085793 | J. Phys. Chem. B XXXX, XXX, XXX−XXX

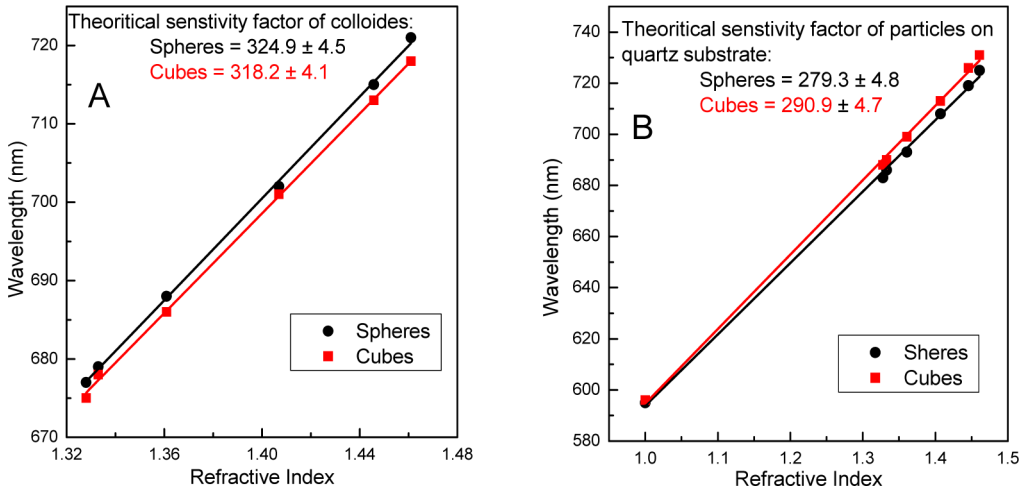

Figure 4. Relationship between the LSPR peak maximum of AuHSs and AuHCs that calculated in different media and the refractive index. (A) The nanoparticles are in the colloid. (B) The nanoparticles are placed on the surface of quartz substrate.

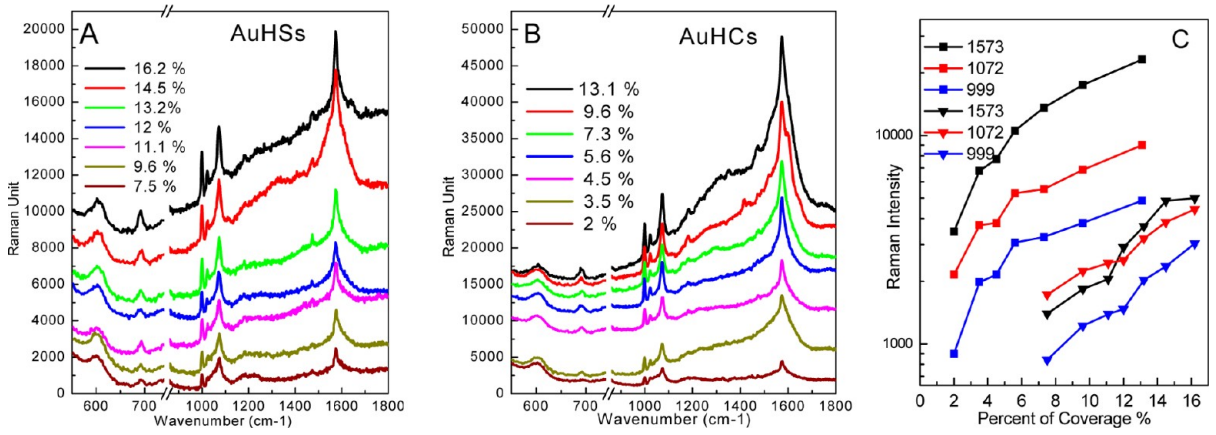

Figure 5. SERS of thiophenol adsorbed on the surface of AuHSs and AuHCs assembled into LB monolayers at different percents of coverage. (A) Hollow gold nanospheres. (B) Hollow gold nanocubes. (C) Relationship between three SERS band intensities of thiophenol and the percent of coverage of AuHSs (triangle symbol) and AuHCs (square symbol).

effect of the substrate on their sensitivity factor values, we carried out discrete dipole approximation (DDA) simulation. The LSPR spectrum of the nanoparticles on a quartz substrate and in colloidal solutions of different surrounding media including methanol, water, ethanol, THF, chloroform, and carbon tetrachloride were calculated. The calculations were used to determine the scattering to absorption ratios as well as the plasmon field intensity. A DDA shape file was prepared to mimic the experimentally prepared hollow gold nanoparticles. The shape file of the AuHSs consisted of a hollow spherical shape (30 nm diameter and 4 nm wall thickness) with four square shaped holes (6 × 6 nm) upon a substrate of 4 nm thickness. The DDA shape file of the AuHCs consisted of a hollow cubical shape (30 nm side length and 5 nm wall thickness) with six square shaped holes (6 × 6 nm) upon a 5 nm thick substrate. The shape files had dipole densities of one dipole per one nanometer. The hole characteristics and nanoparticle orientation on the substrate described in the shape files were chosen to give results that are in agreement with the experimental results. There are two reasons for choosing these shape files (number of holes and the way that the nanoparticles is placed on the surface of the substrate): the first is that the calculation using this shape files gives results in agreement with the experimental results. In fact, several trials for the shape file designation are tested via changing the number of holes and the ways that the nanoparticles are placed on the substrate surface until we obtained agreement with experiments. The observed effect of the substrate is found to agree with the experiment if the AuHS is placed on the substrate through the hole. This is probably due to fact that the side of the nanosphere with the hole is less round (compared to the nanosphere) as well as having more roughness with more valency unsaturated atoms that would be available for strong bonding. This might also explain the observed higher substrate effect on the AuHSs than the AuHCs.

Figure 4A shows the linear relationship between the LSPR maximum peak positions of colloidal AuHSs and AuHCs calculated by DDA simulation and the refractive index of the surrounding medium. The SF values were obtained by calculating the slopes of these lines. For AuHS colloids the SF was 324 ± 4 and for AuHC, 318 ± 4. Similar calculations were carried out for AuHSs and AuHC placed at 1 nm gap from the surface of a quartz substrate. In this case, we calculated the LSPR of the particles in air as well as solvent. The LSPR peak position-refractive index relationship of AuHSs and AuHCs placed on a quartz substrate shown in Figure 4B. In accordance with the experimental results, the substrate decreased the sensitivity factors of AuHS and AuHC by 14 and 8.5%,

dx.doi.org/10.1021/jp3085793 | J. Phys. Chem. B XXXX, XXX, XXX−XXX

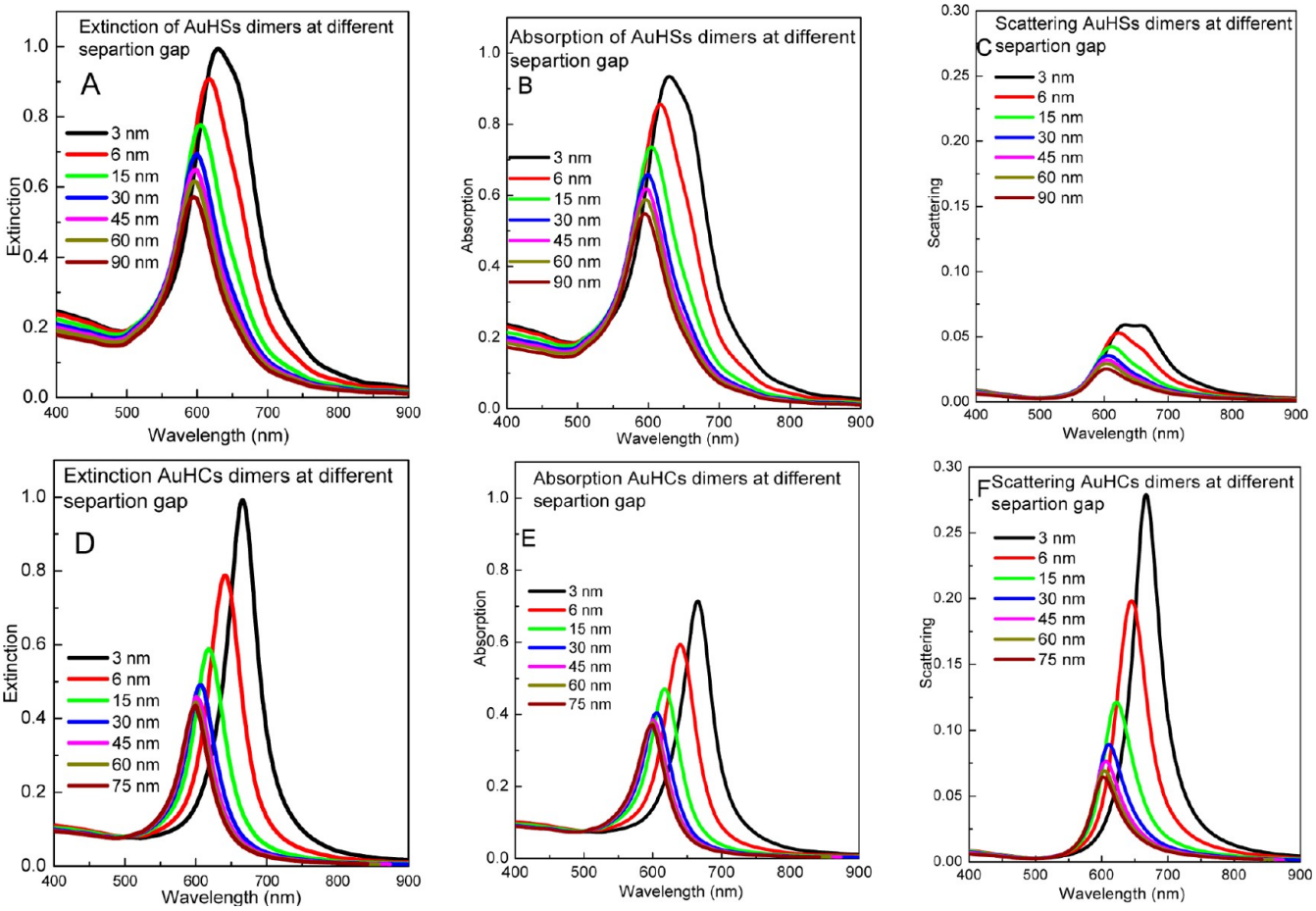

Figure 6. DDA simulation of the LSPR extinction, absorption, and scattering of single AuHSs and AuHCs and dimers placed on the surface of quartz substrate at different separation gaps. (A)−(C) are the extinction, absorption, and scattering of AuHSs, respectively. (D)−(F) are the extinction, absorption, and scattering of AuHCs.

respectively. Similar to the experimental measurements, the AuHSs were affected by the substrate more than the AuHCs, although the contact area of the AuHC with the substrate is higher than the AuHSs.

Comparing Sensing Abilities of AuHCs and AuHSs on the Quartz Substrate by Using SERS. The LSPR extinction spectrum has contributions from the absorption and scattering cross sections with different ratios. In most nanoparticle shapes, the absorption and scattering peaks overlap one another and separate when either the particle size increases or the dielectric function of the medium increases.[9] Therefore, for sensing by LSPR measurement, small plasmonic nanoparticles with low scattering values are more preferable, because when the dielectric function of the surrounding medium increases, the LSPR peaks become broad. As previously reported by our group, the response of the scattering peak to the change of the dielectric function of the surrounding is higher than the absorption peak.[9] This leads to broadening of the LSPR peak with increasing dielectric function, which decreases the accuracy of peak position measurement as well as the slope and especially the value of the figure-of-merit (which is the ratio between the SF and the full width at half-maximum of LSPR peak in electronvolt unit).

The effect of the hollow gold nanoparticles shape on the SERS sensing efficiency is examined by measuring the SERS spectra signal of thiophenol adsorption on their surfaces. Figure 5A shows the SERS of thiophenol adsorbed on the surface of AuHSs LB monolayer assembled on the surface of quartz substrate at different percents of coverage, whereas Figure 5B shows the Raman enhancement of the thiophenol adsorbed on the surface of AuHCs with different percents of coverage. In both, the two nanoparticles monolayers, as the percent of coverage of the nanoparticles increases, the SERS band intensities increase. Figure 5C shows the relationship between the SERS band intensities of thiophenol adsorbed on the surface of AuHSs and AuHCs and their percent of coverage. In the case of AuHSs, the relationship between the logarithm of SERS band intensities and their percent of coverage area seems to be linear. This means that the effect of increasing the percent of coverage of AuHSs does not have any great effect on the Raman enhancement of thiophenol. However, the increase in the SERS bands intensities of thiophenol is due to the concentration effect rather than plasmonic coupling. For AuHCs, the SERS intensities increase with increasing coverage density, the slope is large at low particle density of coverage but is getting smaller as the percent of coverage increases. This AuHCs follows what has been reported, decreasing the SERS efficiency by gold nanocages[18] and gold nanoframe[22] by aggregating them. Although, the sensitivity factor of the AuHSs is higher than that of AuHCs, the SERS enhancement by the AuHCs is ∼5 times higher than that by the AuHSs. This might be due to the fact that we are observing scattering from molecules between cages. The anisotropy of the field distribution around the cages makes it possible to suggest

dx.doi.org/10.1021/jp3085793 | J. Phys. Chem. B XXXX, XXX, XXX−XXX

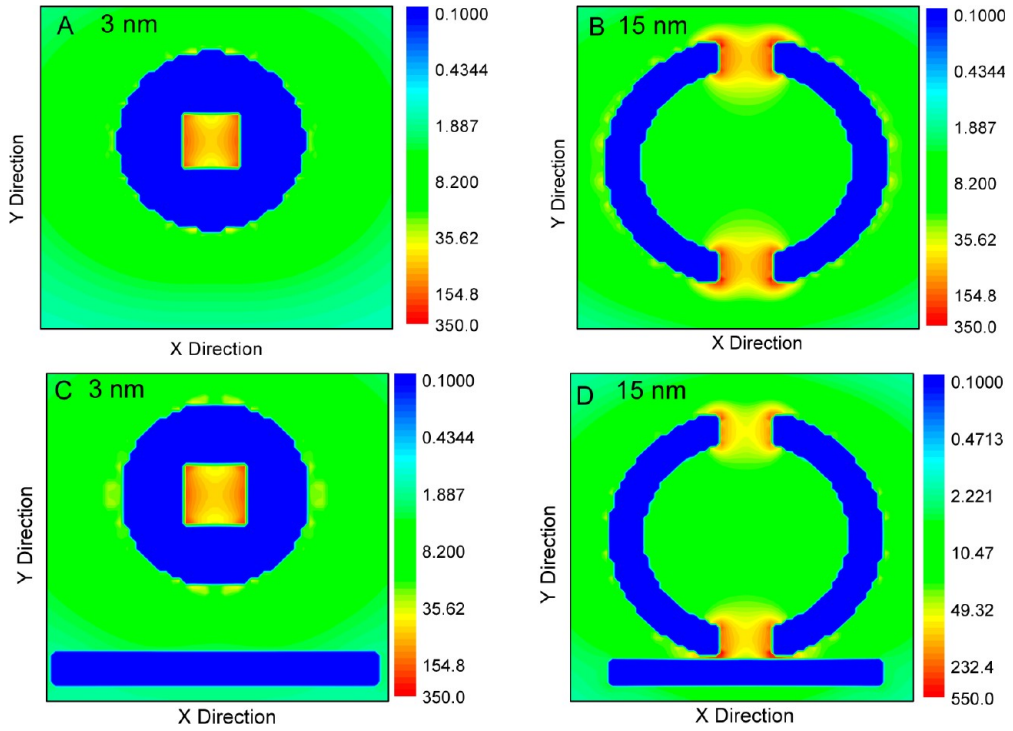

Figure 7. Plasmon field distribution contours of AuHS calculated by DDA simulation. (A) Field distribution on the outer surface around the hole of colloidal AuHS. (B) Field distribution on the middle of colloidal AuHS. (C) Parallel field distribution on the outer surface around the hole of AuHS placed on the surface of quartz substrate. (D) Perpendicular field distribution on the middle of AuHS placed on the surface of quartz substrate.

that we are observing scattering from molecules between cages with their sharp corners facing one another where the plasmonic field is very strong. Moreover, the effective surface area of each AuHS is 55% of the surface area of AuHC. Thus the amount of thiophenol adsorbed on the surface of AuHCs is twice as high as that of AuHSs with the same surface coverage.

DDA Simulation of the LSPR Spectrum of AuHSs and AuHCs at Different Separation Distances. Sensing by plasmonic nanoparticles based on either LSPR or SERS depends on the plasmon field strength and the scattering/absorption ratios. Figure 6A shows the LSPR spectra of single AuHS and AuHC and their dimers placed at 1 nm from a quartz substrate at different separations calculated by the DDA simulation. The separation gaps between the substrate and AuHSs or AuHCs have been taken to be 1 nm on the basis of former results, which showed that the thickness of the PVP capping layer around the gold nanocages is 1 nm.[33] In addition, the best fit between the experiment and theory is obtained when this gap is 1 nm. The LSPR extinction, absorption, and scattering spectra were normalized to the maximum value of extinction peak intensity of the 3 nm separation nanoparticle pair. Although the LSPR peaks shift to lower energy in both AuHSs and AuHCs, five differences were observed: (1) As the separation gap between the nanoparticle dimer decreased, the LSPR peak of AuHSs shifted from 595 to 630 nm, whereas in the case AuHC the shift was from 599 to 666 nm (Figure 3A,D). This result is good accordance with the experimental measurements that showed a large red shift in the LSPR peak of AuHC as the percent of coverage was increased, whereas in the case of AuHSs, the LSPR shift was not significant as the coverage density increased due to the small shift value and the broad LSPR peak (Figure 2). (2) The ratio of scattering to absorption in the case of AuHCs is higher than for AuHSs (Figure 6B–D,F). This indicates that AuHCs have higher SERS efficiency than AuHSs. (3) Hollow gold nanocages of the same size have similar LSPR peak positions if the wall thickness of the spherical shape is thinner than the cubic shape. (4) The absorption band corresponding to the band interband d transition of AuHSs is higher than that of AuHC, which is consistent with the experimental results in Figure 2. The nonradiative decay of the plasmonic excitation occurs via excitation of electron–hole pairs either within the conduction band (intraband excitation) or between the d-band and the conduction band (interband excitations).[12,13] The nonradiative pathways of plasmon decay are responsible for the absorption of light by the nanoparticle. (5) Unlike with the AuHCs, as the separation gap between the AuHSs dimers decreased, the width of the LSPR peak became broader due to the electron oscillation dephasing, which takes place in a short time causing the plasmon field damping. The distribution of the measured energy is expressed by the Lorentzian distribution with a width called the natural line width: fast-decaying of the excitation energy has a broad line width, whereas slow decay has a narrow line width.

Effect of the Substrate on the Plasmon Field Distribution of AuHSs and AuHCs. Although the presented results of the LSPR calculations for the SF of AuHSs and AuHCs both in a colloid and on a substrate supported the experimental measurements, the reason for the decrease of the SF of hollow gold nanoparticles by the quartz substrate could be attributed to the fact that the relative change in the refractive index is less with a substrate present. However, when a colloidal nanoparticle moves from an index of 1.33 in water to an index of 1.46 in chloroform, the medium relative index change is approximately $\Delta n/n = 0.13/1.33 = 0.01$, whereas, when the nanoparticle is on the surface of a quartz substrate (~1.45 index), the effective medium index is higher than 1.33 in water due to the presence of the substrate. Thus the relative change in

dx.doi.org/10.1021/jp3085793 | J. Phys. Chem. B XXXX, XXX, XXX–XXX

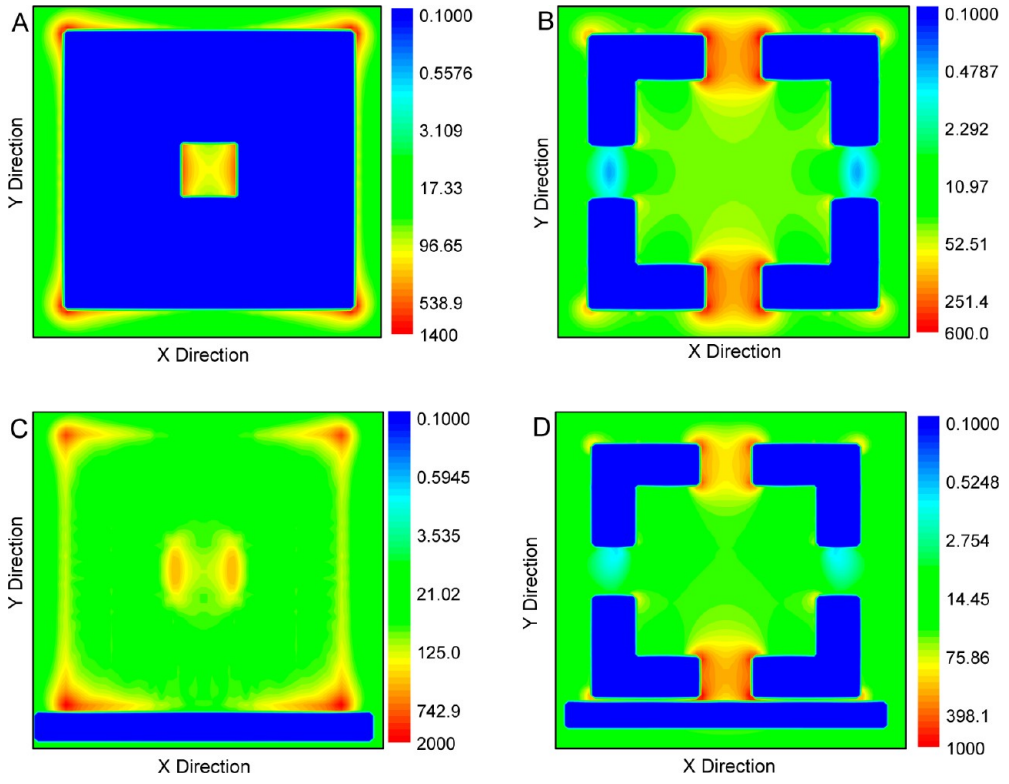

Figure 8. Plasmon field distribution contours of AuHC calculated by DDA simulation. (A) Field distribution on the outer surface around the hole of colloidal AuHC. (B) Field distribution on the middle of colloidal AuHC. (C) Parallel field distribution on the outer surface around the hole of AuHC placed on the surface of quartz substrate. (D) Perpendicular field distribution on the middle of AuHC placed on the surface of quartz substrate.

the effective medium index when the nanoparticles attached to the substrate changes from water to chloroform is less than when the nanoparticles are not attached to the substrate. This is why the sensitivity is seemingly higher when nanoparticles are not attached to the substrate. To confirm this fact, we carried out the plasmon field calculation for gold hollow nanoparticles both in a colloid and on a substrate. Panels A and B of Figure 7 show the plasmon field distribution, calculated by the DDA simulation, on the outer-surface around the hole (3 nm from the outer surface) and in the middle of colloidal AuHS (15 nm from the outer surface), respectively. In the DDA calculations, the light propagates along the *x*-direction and is polarized along the *y*-direction. The plasmon field intensity is high and distributed uniformly on the holes located in the wall of AuHS. Moreover, similar to the solid gold nanosphere,[3] the plasmon field located on the outer surface of AuHS far from the holes has an intensity of 10 times lower than that on the holes. Panels C and D of Figure 7 show the parallel and perpendicular plasmon field distribution of AuHS on the surface of quartz substrate. The plasmon field on the surface of AuHS parallel to the quartz substrate is similar to that of colloidal AuHS (Figure 7C). On the other hand, the plasmon field perpendicular to the substrate is distorted. However, the field intensity close to the surface of the substrate becomes strong at the expense of that on the top of the nanoparticle (Figure 7D). These results explain the reason for the decrease of the sensitivity factor of AuHSs on the surface of quartz substrate. The quartz substrate distorts the plasmon field and weakens the intensity of the field far from the substrate that faces the solvents and strengthens the field close to the substrate.

To show the effect of quartz substrate on the plasmon field distribution intensity and the sensitivity factor of AuHC, DDA calculations were carried out for colloidal AuHC and AuHC on the surface of quartz substrate. Panels A and B of Figure 8 show the plasmon field contour of colloidal AuHC, calculated by the DDA simulation, on both the outer surfaces and in the middle of the particle. Similar to the DDA results of colloidal AuHS, the plasmon field distribution in the outer surface is uniform and the holes have high field intensity, but because AuHC has corners, the plasmon field around the corners is found to be more intense compared with that in the holes. The plasmon field in the interior of the colloidal AuHC is lower than that on the outer surface.

The plasmon field intensity and distribution of AuHC placed on the surface of quartz substrate is shown in Figure 8C,D. The AuHC touches the quartz substrate by one-sixth of its area, which caused distortion of the plasmon field, as in the case of AuHS. The plasmon field distribution close to the quartz substrate is stronger than that away from the substrate. Moreover, the plasmon field intensity far from the substrate is higher than the field intensity of colloidal AuHC. Breaking the symmetry of the plasmon field distribution by the quartz substrate increases the field intensity far and near the substrate. This supported the small decrease in the sensitivity factor value after moving the AuHC on the surface of quartz substrate. The plasmon field intensity of AuHC is higher than the AuHSs in colloid or on a substrate; this is why the SERS enhancement is higher in AuHC. The plasmon field increases near the surface of the substrate; this could be understood to be a result of expected change of the gold electronic coherence due to the increase of the oscillating electrons as a result of the interaction

dx.doi.org/10.1021/jp3085793 | J. Phys. Chem. B XXXX, XXX, XXX−XXX

with the substrate. This is confirmed by the results that showed a red shift in the LSPR peak position of AuHSs and AuHCs, placed on the surface of quartz substrate and surrounded with chloroform, compared with when they are dispersed in chloroform solvent, although the refractive indecies of chloroform and quartz are similar.

Based on the experimental results and the theoretical calculations, the reason for the significant red shift in the LSPR peak of AuHCs with increasing the percent of coverage compared with that of AuHSs is related to the stronger plasmon field coupling between AuNCs compared with AuHSs. The difference in the plasmon filed coupling is due to the following reasons: (1) The area of the AuNCs faces are higher than those of the AuHSs, so the area of coupling is bigger than in AuHCs. (2) The plasmon field of AuNCs is stronger than that of AuHSs; therefore, the plasmon field coupling in the case of AuHCs is stronger than AuHSs.

CONCLUSION

Hollow gold nanospheres and nanocubes of 30 nm were prepared by colloidal chemical methods and assembled into Langmuir−Blodgett monolayers on the surface of quartz substrates at different surface densities. The LSPR of the cubic shape was found to red-shift by increasing the surface density whereas the spherical shape was little affected. DDA calculations for a pair of AuHSs and AuHCs placed on the surface of a quartz substrate at different separation gaps showed that the plasmon coupling in a pair of cubes is higher than that of a pair of spheres. Therefore, when the interparticle distance decreases, the shift of the LSPR spectrum of AuHCs becomes higher than that of AuHSs. This calculation agrees with the experimental results (small shift in the LSPR peaks of AuHSs on increasing the coverage density). Although the sensitivity factor of the studied AuHSs is higher than that of AuHCs both in a colloid and on a substrate, the quality of AuHSs as a LSPR sensor decreases more than that of AuHCs when placed on a substrate. DDA calculations showed that the substrate does not change the plasmon field far from the surface of the substrate in the case of AuHCs whereas it does in AuHSs. Unlike with LSPR sensing efficiency, Au HCs are 5 times more sensitive than AuHSs for SERS sensing. The DDA simulations of the LSPRs showed that AuHCs have a higher scattering cross section than AuHSs, in agreement with the higher Raman enchantment by AuHCs.

ASSOCIATED CONTENT

Supporting Information

SEM images of AuHSs and AuHCs LB monolayers with different densities of coverage are in Figures S1 and S2, respectively. Field enhancement contours of AuHS dimers placed at different separation distances calculated by the DDA calculation are shown in Figures S3−S6. This information is available free of charge via the Internet at http://pubs.acs.org/.

AUTHOR INFORMATION

Corresponding Author

*E-mail: melsayed@gatech.edu.

Notes

The authors declare no competing financial interest.

ACKNOWLEDGMENTS

This work was supported by the Department of Energy grant No. DE-FG02-09ER46604. The authors thank Mr. Daniel O'Neil for his careful proofreading of the manuscript and for his valuable discussion.

REFERENCES

(1) Kreibig, U.; Vollmer, M. *Optical Properties of Metal Clusters*; Springer Series in Materials Science 25; Springer: Berlin, 1995.
(2) Malinsky, M. D.; Kelly, K. L.; Schatz, G. C.; Van Duyne, R. P. *J. Phys. Chem. B* **2001**, *105*, 2343−2350.
(3) Kelly, K. L.; Coronado, E.; Zhao, L. L.; Schatz, G. C. *J. Phys. Chem. B* **2003**, *107*, 668−677.
(4) Malinsky, M. D.; Kelly, K. L.; Schatz, G. C.; Van Duyne, R. P. *J. Am. Chem. Soc.* **2001**, *123*, 1471−1482.
(5) Hao, E.; Schatz, G. C. *J. Chem. Phys.* **2004**, *120*, 357−366.
(6) Freund, P. L.; Spiro, M. *J. Phys. Chem.* **1985**, *89*, 1074−1077.
(7) Haes, A. J.; Zou, S.; Schatz, G. C.; Van Duyne, R. P. *J. Phys. Chem. B* **2004**, *108*, 6961−6968.
(8) Haes, A. J.; Van Duyne, R. P. *J. Am. Chem. Soc.* **2002**, *124*, 10596−10604.
(9) Mahmoud, M. A.; Chamanza, M.; Adibi, A.; El-Sayed, M. A. *J. Am. Chem. Soc.* **2012**, *134*, 6434−6442.
(10) Ringe, E.; McMahon, J. M.; Sohn, K.; Cobley, C.; Xia, Y. N.; Huang, J. X.; Schatz, G. C.; Marks, L. D.; Van Duyne, R. P. *J. Phys. Chem. C* **2010**, *114*, 12511−12516.
(11) Knight, M. W.; Wu, Y.; Lassiter, J. B.; Nordlander, P.; Halas, N. J. *Nano Lett.* **2009**, *9*, 2188−2192.
(12) Sun, Y. G.; Xia, Y. N. *Science* **2002**, *298*, 2176−2179.
(13) Jana, N. R.; Gearheart, L.; Murphy, C. J. *J. Phys. Chem. B* **2001**, *105*, 4065−4067.
(14) Nehl, C. L.; Liao, H. W.; Hafner, J. H. *Nano Lett.* **2006**, *6*, 683−688.
(15) Jin, R.; Cao, Y. C.; Hao, E.; Metraux, G. S.; Schatz, G. C.; Mirkin, C. A. *Nature (London, U. K.)* **2003**, *425*, 487−490.
(16) Oldenburg, S. J.; Averitt, R. D.; Westcott, S. L.; Halas, N. J. *Chem. Phys. Lett.* **1998**, *288*, 243−247.
(17) Schwartzberg, A. M.; Olson, T. Y.; Talley, C. E.; Zhang, J. Z. *J. Phys. Chem. B* **2006**, *110*, 19935−19944.
(18) Mahmoud, M. A.; Snyder, B.; El-Sayed, M. A. *J. Phys. Chem. C* **2010**, *114*, 7436−7443.
(19) Mahmoud, M. A.; El-Sayed, M. A. *J. Am. Chem. Soc.* **2010**, *132*, 12704−12710.
(20) Nie, S. M.; Emery, S. R. *Science* **1997**, *275*, 1102−1106.
(21) Draine, B. T.; Flatau, P. J. *J. Opt. Soc. Am. A-Opt. Image Sci. Vis.* **1994**, *11*, 1491−1499.
(22) Mahmoud, M. A.; El-Sayed, M. A. *Nano Lett.* **2009**, *9*, 3025−3031.
(23) Reinhard, B. M.; Siu, M.; Agarwal, H.; Alivisatos, A. P.; Liphardt, J. *Nano Lett.* **2005**, *5*, 2246−2252.
(24) Zhao, J.; Zhang, X. Y.; Yonzon, C. R.; Haes, A. J.; Van Duyne, R. P. *Nanomedicine* **2006**, *1*, 219−228.
(25) Hall, W. P.; Ngatia, S. N.; Van Duyne, R. P. *J. Phys. Chem. C* **2011**, *115*, 1410−1414.
(26) Huang, C. C.; Yang, Z.; Lee, K. H.; Chang, H. T. *Angew. Chem., Int. Ed.* **2007**, *46*, 6824−6828.
(27) Tabor, C.; Murali, R.; Mahmoud, M.; El-Sayed, M. A. *J. Phys. Chem. A* **2009**, *113*, 1946−1953.
(28) Tao, A.; Kim, F.; Hess, C.; Goldberger, J.; He, R.; Sun, Y.; Xia, Y.; Yang, P. *Nano Lett.* **2003**, *3*, 1229−1233.
(29) Mahmoud, M. A.; Tabor, C. E.; El-Sayed, M. A. *J. Phys. Chem. C* **2009**, *113*, 5493−5501.
(30) Solis, D.; Willingham, B.; Nauert, S. L.; Slaughter, L. S.; Olson, J.; Swanglap, P.; Paul, A.; Chang, W. S.; Link, S. *Nano Lett.* **2012**, *12*, 1349−1353.
(31) Aslan, K.; Lakowicz, J. R.; Geddes, C. D. *Curr. Opin. Chem. Biol.* **2005**, *9*, 538−544.

(32) Wokaun, A.; Gordon, J. P.; Liao, P. F. *Phys. Rev. Lett.* **1982**, *48*, 957−960.
(33) Mahmoud, M. A.; El-Sayed, M. A. *J. Phys. Chem. C* **2011**, *115*, 12726−12735.
(34) Tao, A.; Sinsermsuksakul, P.; Yang, P. *Nat. Nanotechno.l* **2007**, *2*, 435−440.